MICROSCOPY

*Microscopy* **62(Supplement 1)**: S87–S98 (2013)
doi: 10.1093/jmicro/dft014

Article

# Interpretation of phase images of delta-doped layers

David Cooper[1] and Rafal E. Dunin-Borkowski[2,*]

[1]CEA-LETI, Minatec Campus, 17 rue des Martyrs, F-38054 Grenoble Cedex 9, France and [2]Ernst Ruska-Centre for Microscopy and Spectroscopy with Electrons and Peter Grünberg Institute, Forschungszentrum Jülich, D-52425 Jülich, Germany
*To whom correspondence should be addressed. E-mail: rdb@fz-juelich.de

**Abstract** An approach is presented that allows independent determination of the mean inner potential contribution to a phase image of a highly doped layer in a semiconductor measured using off-axis electron holography, in order to quantify the contribution to the recorded phase from the dopant potential alone. The method takes into account the possible presence of both substitutional and interstitial dopant atoms and is used here to analyse an experimental phase image of 12 delta-doped B layers in Si that are separated from each other by <6 nm.

**Keywords** off-axis electron holography, electrostatic potential, mean inner potential, dopant potential, delta-doping, semiconductor

**Received** 27 January 2013, accepted 2 March 2013; online 26 March 2013



## Introduction

Off-axis electron holography in the transmission electron microscope (TEM) is a powerful technique for the measurement of magnetic fields and electrostatic potentials in materials [1–4]. The technique typically requires the use of a microscope equipped with a field emission electron gun and an electron biprism to interfere part of the electron wave that has passed through a region of interest on the specimen with another part of the same electron wave that has passed through a field-free region of space, in order to form an interference fringe pattern or electron hologram. The interference fringes in the electron hologram can be interpreted to obtain real-space images of both the amplitude and the phase shift of the electron wave that has passed through the specimen. The phase shift is of particular interest, because it is sensitive to the in-plane magnetic induction and the electrostatic potential within and around the specimen.

For a non-magnetic specimen, the phase shift is given by the expression

$$\phi(x,y) = C_E \int V(x,y)\,\mathrm{d}z, \qquad (1)$$

where $V$ is the electrostatic potential, $z$ is the incident electron beam direction and $C_E$ is a constant that takes a value of $7.29\times10^6\,\mathrm{rad\,V^{-1}\,m^{-1}}$ at a microscope accelerating voltage of 200 kV. The primary contribution to $V$ is usually the mean inner potential of the specimen, which is sensitive to its local composition and density, and is given by the expression

$$V_0 = \left(\frac{h^2}{2\pi m e\,\Omega}\right)\sum_{\Omega} f_{\mathrm{el}}(0) \equiv \left(\frac{k}{\Omega}\right)\sum_{\Omega} f_{\mathrm{el}}(0), \qquad (2)$$

where $k = 4.7878\times10^{-19}\,\mathrm{J\,m^2\,C^{-1}}$ and $f_{\mathrm{el}}(0)$ is the electron scattering factor at zero scattering angle of each atom in volume $\Omega$.

In a doped semiconductor, an additional contribution to $V$ is associated with the dopant potential [5–12], whose characterization using electron holography is important for the semiconductor industry and requires the preparation of TEM specimens of highly uniform thickness, whose electrical properties are affected minimally by TEM specimen preparation from those in the bulk device. If these criteria are met, if the specimen thickness is known

independently, if the specimen is sufficiently thick that the effect on the phase of surface depletion is minimal and if specimen charging and dynamical diffraction are negligible, then variations in dopant potential in the specimen can in principle be measured quantitatively from a recorded phase image.

Most previous studies of dopant potentials in semiconductors using electron holography have involved the examination of specimens in which the dopant concentration is low enough (below $\sim 10^{19}$ $cm^{-3}$) that local variations in dopant species and/or concentration could not be discerned in a bright-field or dark-field TEM image. However, in some of the most modern semiconductor devices, the dopant concentration is sufficiently high that there may be two significant contributions to the phase change associated with the dopants in the specimen: one originating from the dopant potential of primary interest and one from local variations in mean inner potential. A further complication is related to the fact that the dopant may no longer be fully substitutional or electrically active. The application of electron holography to such specimens, therefore, requires not only the use of a highly stable microscope and long acquisition times to measure small changes in phase with high spatial resolution [13,14], but also the separation of the dopant potential from contributions to the measured potential that are associated with changes in local scattering factor and density [15–17].

Here, we show how the mean inner potential contribution to a phase image of a very highly doped semiconductor can be determined independently in order to interpret the dopant potential in the specimen. We illustrate the method through the examination of a series of B delta-doped layers in Si, each of which is intended to comprise a narrow layer of dopant atoms (thinner than a few unit cells) and a space charge layer of opposite sign that extends on either side of it [18].

## Methods

The specimen analysed in the present study was grown on (001) Si using reduced pressure chemical vapour deposition and contained 12 closely spaced delta-doped layers of B in Si. A secondary ion mass spectrometry (SIMS) profile acquired from the layers is shown in Fig. 1. The layers that are labelled 1–5 in the SIMS profile, which are closest to the wafer surface, are nominally 3.5 nm apart, while the subsequent layers are nominally 6.0 nm apart. The peaks in the SIMS profile reach concentrations of up to $3 \times 10^{21}$ $cm^{-3}$, which is equivalent to ~6% B on a Si lattice and is much higher than the solubility limit reported for delta-doped layers of B in Si of $6 \times 10^{20}$ $cm^{-3}$ [19]. The width of each of the layers $w$, measured as a full-width at half-maximum (fwhm) directly from the SIMS profile, is given in Table 1 and has an average value of $1.62 \pm 0.06$ nm. As a result of the poor lateral spatial resolution of SIMS and other artefacts associated with the technique, the local B concentration in each layer is expected to exceed the measured value of $3 \times 10^{21}$ $cm^{-3}$ and each layer is expected to be narrower than the value of 1.62 nm measured using SIMS.

Focused ion beam (FIB) milling with Ga ions at 8 kV was used to prepare parallel-sided specimens of the delta-doped layers for TEM examination, taking great care to avoid introducing physical damage or implantation of Ga. Off-axis electron holograms, high-resolution TEM images and high-angle annular dark-field (HAADF) scanning TEM (STEM) images were acquired at 200 kV using an FEI Titan TEM. A specimen of nominal thickness 250 nm was used for electron holography and for high-resolution TEM, while a specimen of nominal thickness 150 nm was used for HAADF STEM. The true 'crystalline' thickness of the nominally 250-nm-thick specimen was measured to be 245 nm from a convergent beam electron diffraction pattern acquired in a two-beam 004 diffracting condition, with the specimen oriented ~5° from the <110> zone axis. The estimated precision of this measurement was ±2 nm.

Off-axis electron holograms of the layers were acquired using a biprism voltage of 55 V and an acquisition time of 64 s, with the specimen tilted by a few degrees from <110> in order to minimize the effects of dynamical diffraction, while maintaining the layers close to vertical. As a result of the narrow spacings and the widths of the layers, values of ~80 and 0.33 nm were chosen for the overlap width and interference fringe spacing in each hologram, respectively, by operating the

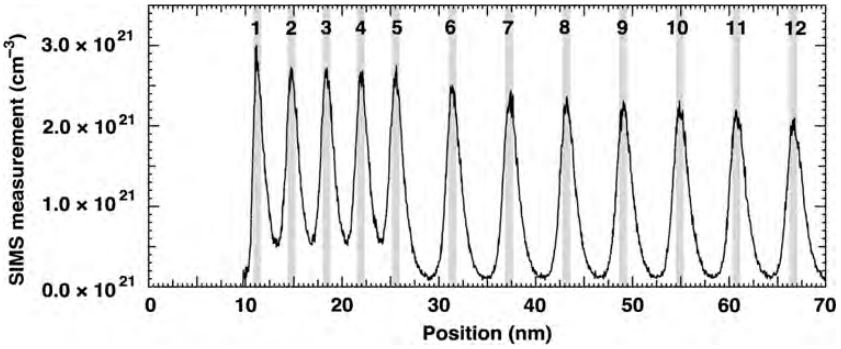


**Fig. 1.** SIMS-measured B concentration profile measured from the 12 delta-doped layers in Si studied here. Layer 1 is closest to the wafer surface. The average separations between layers 1–5 and 5–12 are measured to be 3.57 and 5.85 nm, respectively, from the high-resolution TEM and STEM images shown in Fig. 4a and c. The total B content $n_B$ and the width $w$ (full-width at half-maximum) of each delta-doped layer, measured directly from the SIMS profile, are given in Table 1. The true positions of the layers (also determined from the high-resolution TEM and STEM images) are marked using vertical grey lines.

**Table 1.** Total B content $n_B$ (expressed as an equivalent number of atomic layers if the B atoms were all placed on a Si lattice) and width $w$ (full-width at half-maximum) of each delta-doped layer measured from the SIMS profile shown in Fig. 1

| Layer number | Total B content $n_B$ in layer measured using SIMS | Layer width $w$ measured using SIMS (nm) |
|---|---|---|
| 1 | 0.63 | 1.22 |
| 2 | 0.74 | 1.37 |
| 3 | 0.75 | 1.43 |
| 4 | 0.73 | 1.45 |
| 5 | 0.77 | 1.45 |
| 6 | 0.73 | 1.72 |
| 7 | 0.72 | 1.76 |
| 8 | 0.70 | 1.74 |
| 9 | 0.71 | 1.77 |
| 10 | 0.70 | 1.84 |
| 11 | 0.70 | 1.86 |
| 12 | 0.68 | 1.88 |
| Average | 0.71 | 1.62 |
| Standard error in mean | 0.01 | 0.06 |

The value of $n_B$ for each layer was determined by integrating each peak in the SIMS profile numerically between adjacent minima in Fig. 1. The average value of each parameter is also given.

microscope with the Lorentz lens switched off and the intermediate and diffraction lenses partially excited using the free lens control mode of the microscope. A vacuum reference hologram was acquired after each specimen hologram to remove distortions associated with the imaging and recording system of the microscope. High-resolution TEM and HAADF STEM images were acquired with the specimen oriented exactly at the <110> zone axis using a 50 µm objective aperture and a 115 mm camera length, respectively. Measurements of the rigid shift (i.e. expansion or contraction) of the Si lattice across each layer relative to unstrained Si were obtained by applying geometrical phase analysis (GPA) [20] to a recorded HAADF STEM image. This approach proved to be more reliable than applying GPA to a high-resolution TEM image or to using dark-field electron holography or nanobeam electron diffraction.

The approach that we introduce here to determine the mean inner potential contribution to the phase shift of a delta-doped layer involves obtaining complementary information about the specimen from the SIMS profile shown in Fig. 1 and from an HAADF STEM image. As neither the ratio of substitutional to interstitial B in each layer nor the proportion of B that is electrically active is known, we suggest that both of these quantities should subsequently be inferred from the (total) recorded phase shift by making use of process simulations to calculate the dopant potential profile that would be consistent with both the independently measured mean inner potential profile and the total potential profile measured from the original experimental phase image. Here, we address only the determination of the mean inner potential contribution to the phase. The use of process simulations to infer the dopant potential contribution will be described elsewhere.

Our approach relies on the determination of three parameters for the same delta-doped layer that is examined using electron holography. The first parameter is $n_B$, the total amount of B in each layer, which is determined here from the SIMS profile shown in Fig. 1. For convenience, we choose to

express $n_B$ in the form of an equivalent number of atomic layers if the B atoms were all placed on a Si lattice. The second parameter is $w$, the compositional width of the layer, which is measured here from an HAADF STEM image. The third parameter is $d_c$, the total rigid shift (i.e. expansion or contraction) of the Si lattice across the layer relative to a perfect unstrained Si lattice, measured using GPA.

We begin by defining the total number of atomic layers in the delta-doped layer in the form:

$$n_T = \left(\frac{w + d_c}{a_{Si}/4}\right), \quad (3)$$

where $d_c$ is chosen here to be positive for a contraction of the Si lattice across the layer (as would be expected for substitutional B), as shown schematically in Fig. 2. By combining Eqs. (2) and (3), the mean inner potentials of the layer and the Si lattice can be written in the form:

$$V_0(\text{layer}) = k\left(\frac{(n_T - xn_B) f_{Si} + n_B f_B}{a_0^2 w}\right), \quad (4)$$

$$V_0(\text{Si}) = k\left(\frac{n_T f_{Si}}{a_0^2 (w + d_c)}\right), \quad (5)$$

where $x$ is the fraction of B in the layer that is substitutional and $f_{Si}$ and $f_B$ are electron scattering factors at zero scattering angle for Si and B, respectively. The fractional change in mean inner potential from that of the Si lattice is then given by the expression:

$$\frac{\Delta V_0}{V_0} = \left(\frac{V_0(\text{layer}) - V_0(\text{Si})}{V_0(\text{Si})}\right) = \left(\frac{w + d_c}{w}\right)\left[\frac{(n_T - xn_B) f_{Si} + n_B f_B}{n_T f_{Si}}\right] - 1. \quad (6)$$

By making use of Eq. (3), $n_T$ can be eliminated from Eq. (6) to give the final equation:

$$\frac{\Delta V_0}{V_0} = \left(\frac{d_c}{w}\right) + n_B\left(\frac{a_{Si}}{4w}\right)\left(\frac{f_B}{f_{Si}} - x\right), \quad (7)$$

which can be used to infer a value for $\Delta V_0$ from experimental measurements of $n_B$, $w$ and $d_c$ if $V_0$, $f_{Si}$ and $f_B$ are known.

It should be noted that some care is required to ensure that the same contribution to the total potential is not counted twice. Specifically, the change in electron scattering factor (from neutral atom values) that results from the ionization of substitutional dopant atoms (and from the spatial separation of the resulting free charge from these ions) is ultimately likely to be equivalent to the dopant potential. Therefore, neutral and not ionic scattering factors are used below to determine the local

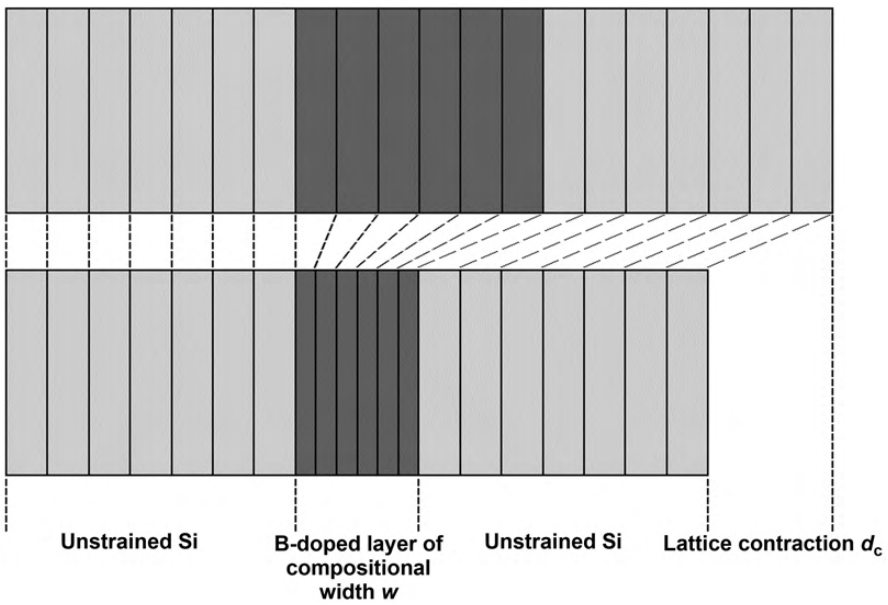


**Fig. 2.** Schematic diagram illustrating the nature of the expected rigid shift of the Si lattice $d_c$ that is assumed to be present across a delta-doped layer of width $w$ as a result of the different lattice parameter of the layer from that of pure unstrained Si in the growth direction. The diagram shows a lattice contraction, i.e. a layer that has a smaller lattice parameter in the growth direction than unstrained Si.

change in mean inner potential, on the assumption that the dopant potential takes into account all of the contributions to the potential that are associated with longer-range redistribution of free (space) charge from bound (electrically active) substitutional B.

## Results

In this section, values of the change in potential at the 12 delta-doped layers examined here are measured using off-axis electron holography and compared with mean inner potential contributions to the potential, which are inferred from independent SIMS and HAADF STEM measurements of $n_B$, $w$ and $d_c$ using Eq. (7).

Figure 3a and c shows selected regions of experimental phase and amplitude images, respectively, recorded using off-axis electron holography from the 12 delta-doped layers studied here. There are two very significant observations. First, the presence of dark contrast at the position of each layer in the amplitude image indicates that changes in composition and density (i.e. mean inner potential) are likely to be sufficiently strong to influence the phase image. Second, the layers are visibly wider in the phase image than in the amplitude image, suggesting that the contrast in the phase image contains a significant contribution from the dopant potential, which is expected to be wider than the compositional width of each layer. Corresponding line profiles are shown in Fig. 3b and d, while the measured changes in phase and widths of the layers are given in Table 2. The average change in phase at the position of each layer is $-0.23 \pm 0.01$ radians, which corresponds to a total change in potential of $-0.126 \pm 0.005$ V according to Eq. (1) on the assumption that the specimen thickness is 245 nm and that electrically inactive specimen surface layers can be neglected. The latter assumption has been shown to be reasonable for a very high doping concentration [21]. The average widths of the phase and amplitude profiles across the layers are $2.30 \pm 0.04$ nm and $1.62 \pm 0.08$ nm, respectively. The interpretation of the line profiles shown in Fig. 3b and d and the values listed in Table 2 forms the basis for the following analysis and discussion.

It is also important to note that a lower magnification electron hologram (not shown here), which was acquired with a larger field of view in Lorentz mode using a 2.2 nm interference fringe spacing, indicated that the region of the layers shown in Fig. 3 has a 0.62 V lower potential than the Si substrate, with the potential increasing just outside the field of view on the right-hand side of Fig. 3a and b. The rise in potential at the edges of the 12 layers is also responsible for the fact that it was not possible to measure the width or the depth of the change in phase for layer 1 or 2 (see Fig. 3 and Table 2), where the phase profile rises rapidly towards the original wafer surface.

The first parameter that is required for an independent determination of the mean inner potential contribution to the measured potential is the total amount of B in each layer, $n_B$. This value was determined here by integrating each peak in the SIMS profile shown in Fig. 1 numerically, which results in an average value for $n_B$ of $0.71 \pm 0.01$, as given in Table 1.

The second parameter that is required is the compositional layer width, $w$. Figure 4 shows high-resolution TEM and STEM images of the delta-doped layers and corresponding line profiles. Interestingly, the layers appear dark in both images. Measurements of the width of each layer from the line profiles are given in Table 3 and take average values of $1.08 \pm 0.07$ and $1.16 \pm 0.01$ nm from the high-resolution TEM and STEM images, respectively. The difference between these values is not significant for the conclusions presented below, and the value of $w$ determined from the HAADF STEM image is used in the determination of the mean inner potential contribution to the total potential. Based on the known lattice parameter of the Si substrate, the images also show that the true values of the narrower and wider spacings between the layers are, on average, 3.57 and 5.85 nm, respectively.

At this point, the possibility that there is a slight broadening of the layer profiles measured using electron holography, resulting from several factors that may include filtering of the highest spatial frequencies in the sideband, undersampling of the phase image and the use of a slight tilt of the layers from the vertical orientation to avoid the effects of dynamical diffraction, can be considered. It was

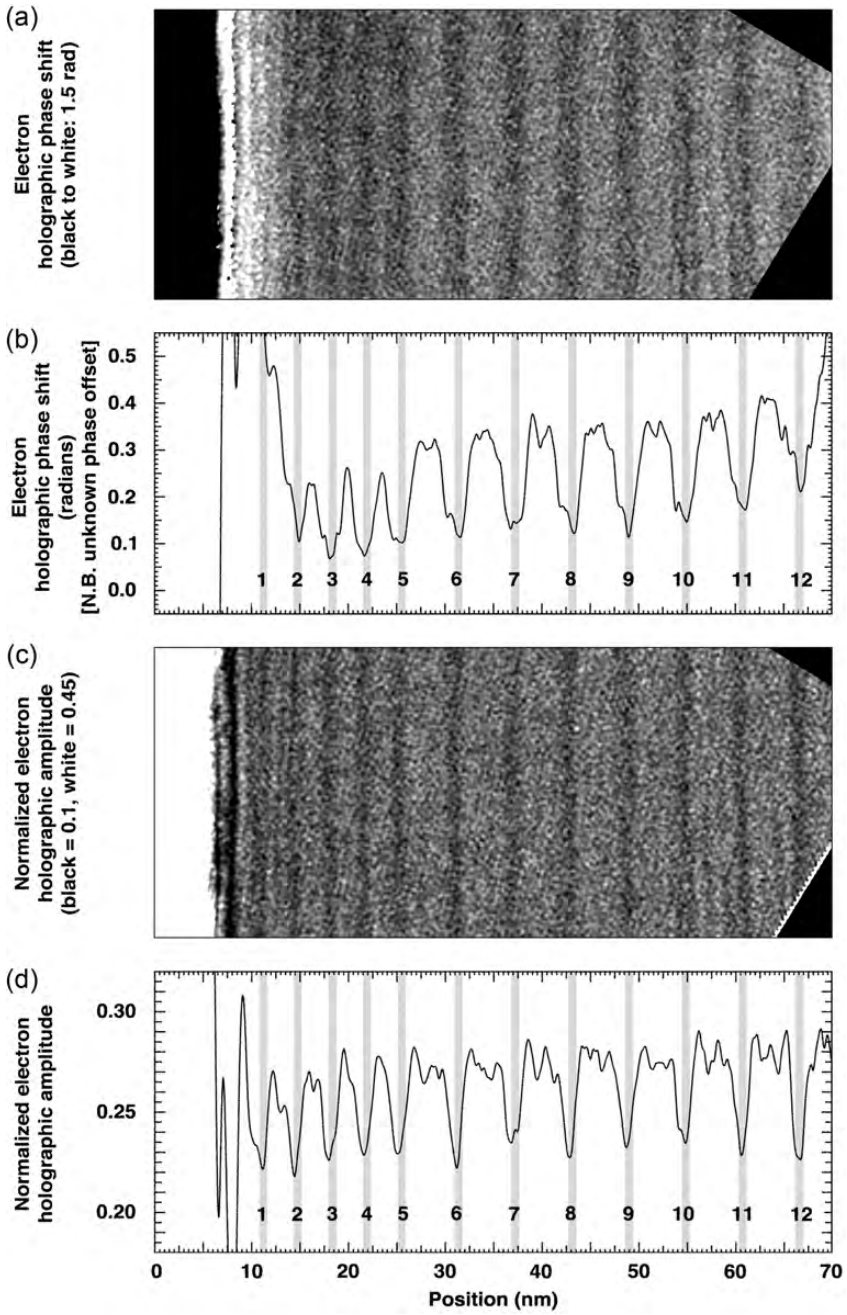


**Fig. 3.** (a) Part of a phase image reconstructed from an off-axis electron hologram recorded from the layers using an interference fringe spacing of 0.33 nm (black to white = 1.5 rad). (b) Line profile obtained by projecting the phase image along the layers. The vertical scale is in radians, but has an unknown additive constant as the phase in vacuum was not recorded in the same image. (c) Part of an amplitude image reconstructed from the same off-axis electron hologram (black = 0.1, white = 0.45). (d) Line profile obtained by projecting the amplitude image along the layers. The specimen was tilted a few degrees away from the <110> zone axis during hologram acquisition, while keeping the layers close to vertical. A vacuum reference hologram was used to remove phase distortions from the imaging and recording system of the microscope, as well as to normalize the amplitude image to a level of unity in vacuum. The layers on the extreme right- and left-hand sides of the images show additional faint fringes, which are artefacts introduced by Fresnel fringes from the edges of the biprism wire but do not affect the line profiles significantly. Note that the contrast from each layer is narrower in the amplitude image and line profile than in the phase image and line profile. The positions of the layers are marked in grey on each line profile.

determined that deconvolution of the electron holographic amplitude image using a Gaussian peak of width 1.15 nm results in a match between the average value of layer width $w$ measured from the amplitude image and that measured from the HAADF STEM image. The application of the same

**Table 2.** Depth $\Delta\phi$ and width $w$ (full-width at half-maximum) of each delta-doped layer measured from the electron holographic phase profile shown in Fig. 3b and width $w$ (full-width at half-maximum) of each delta-doped layer measured from the electron holographic amplitude profile shown in Fig. 3d

| Layer number | Well depth $\Delta\phi$ measured from phase (radians) | Layer width $w$ measured from phase (nm) | Layer width $w$ measured from amplitude (nm) |
|---|---|---|---|
| 1 | – | – | – |
| 2 | – | – | – |
| 3 | –0.18 | 2.39 | 1.5 |
| 4 | –0.19 | 2.08 | 1.43 |
| 5 | –0.19 | 2.08 | 1.77 |
| 6 | –0.23 | 2.31 | 1.54 |
| 7 | –0.24 | 2.35 | 1.5 |
| 8 | –0.25 | 2.31 | 1.77 |
| 9 | –0.25 | 2.39 | 2.12 |
| 10 | –0.25 | 2.43 | 1.5 |
| 11 | –0.29 | 2.35 | 1.43 |
| 12 | – | – | – |
| Average | –0.23 | 2.30 | 1.62 |
| Average after deconvolution by gaussian peak of width 1.15 nm | –0.265 | 2.0 | 1.16 |
| Standard error in mean | 0.01 | 0.04 | 0.08 |

The average value of each parameter is also given, both before and after deconvolution of the phase and amplitude profiles using a Gaussian peak of width 1.15 nm, in order to achieve consistency between the layer widths $w$ measured from the amplitude profile and a high-resolution STEM image profile (see Fig. 4d and Table 3), i.e. to take into account effects such as a slight tilt of the layers from the vertical during electron hologram acquisition.

**Table 3.** Width $w$ (full-width at half-maximum) of each delta-doped layer measured from the high-resolution TEM and STEM image profiles in Fig. 4b and d, respectively

| Layer number | Layer width $w$ measured from high-resolution TEM image (nm) | Layer width $w$ measured from high-resolution STEM image (nm) | Lattice expansion $d_c$ across layer measured from high-resolution STEM image (nm) |
|---|---|---|---|
| 1 | – | 1.13 | –0.0161 |
| 2 | 1.12 | 1.12 | –0.0161 |
| 3 | 1.04 | 1.17 | –0.0124 |
| 4 | 1.27 | 1.09 | –0.0158 |
| 5 | 1.38 | 1.18 | –0.0209 |
| 6 | 1.5 | 1.18 | –0.0263 |
| 7 | 1.25 | 1.13 | –0.0258 |
| 8 | 0.9 | 1.19 | –0.0183 |
| 9 | 0.89 | 1.16 | –0.0277 |
| 10 | 0.78 | 1.22 | –0.0227 |
| 11 | 0.9 | 1.19 | –0.0295 |
| 12 | 0.83 | 1.18 | –0.0175 |
| Average | 1.08 | 1.16 | –0.0208 |
| Standard error in mean | 0.07 | 0.01 | 0.0016 |

The right-hand column shows the rigid expansion of the Si lattice across each layer, measured from the integrated strain profile shown in Fig. 5d. The average value of each parameter is also given.

deconvolution procedure to the phase image results in corrected values of –0.265 rad and 2.0 nm for the average depth and width of the phase profile across each layer, respectively, corresponding to a corrected change in total potential of –0.148 V if the measured value for the specimen thickness of 245 nm is used. It should be noted that, if this were the only origin, a broadening by 1.15 nm in a specimen of thickness 245 nm would result from a specimen tilt of the layers from the vertical by 0.27°.

The third parameter that is required is the rigid shift (i.e. expansion or contraction) $d_c$ of the Si lattice, relative to unstrained Si, across each layer. This parameter was determined by applying GPA to the HAADF STEM image shown in Fig. 4c to provide a map of the strain in the growth direction of the layers, which is shown in Fig. 5a. A corresponding line profile of the strain, obtained by projecting Fig. 5a along the layers, is shown in Fig. 5b. Interestingly, the average value of the strain at each layer is positive, corresponding to an expansion of the Si lattice relative to unstrained Si, whereas a contraction of the lattice would be expected for fully substitutional B [22,23]. This observation provides further evidence for the presence of a substantial proportion of interstitial B, which has been reported to cause a lattice expansion in Si [19]. On the assumption that the Si lattice between each layer is unstrained, and in particular in order to take into account low-frequency artefacts in the HAADF STEM image introduced by scan distortions and slight specimen drift, a slowly varying background was subtracted from the strain profile to produce the corrected profile shown in Fig. 5c. This corrected strain profile was then integrated from its left-hand side to determine the cumulative lattice expansion across the layers, as shown in Fig. 5d. Based on this profile, the average value of the expansion of the Si lattice resulting from the presence of each delta-doped layer $d_c$ is inferred to be $-0.0208 \pm 0.0016$ nm, which corresponds to 15% of the spacing of one atomic layer in Si along 001. It should be noted that no misfit dislocations, which could affect the strain profile, were observed in this specimen.

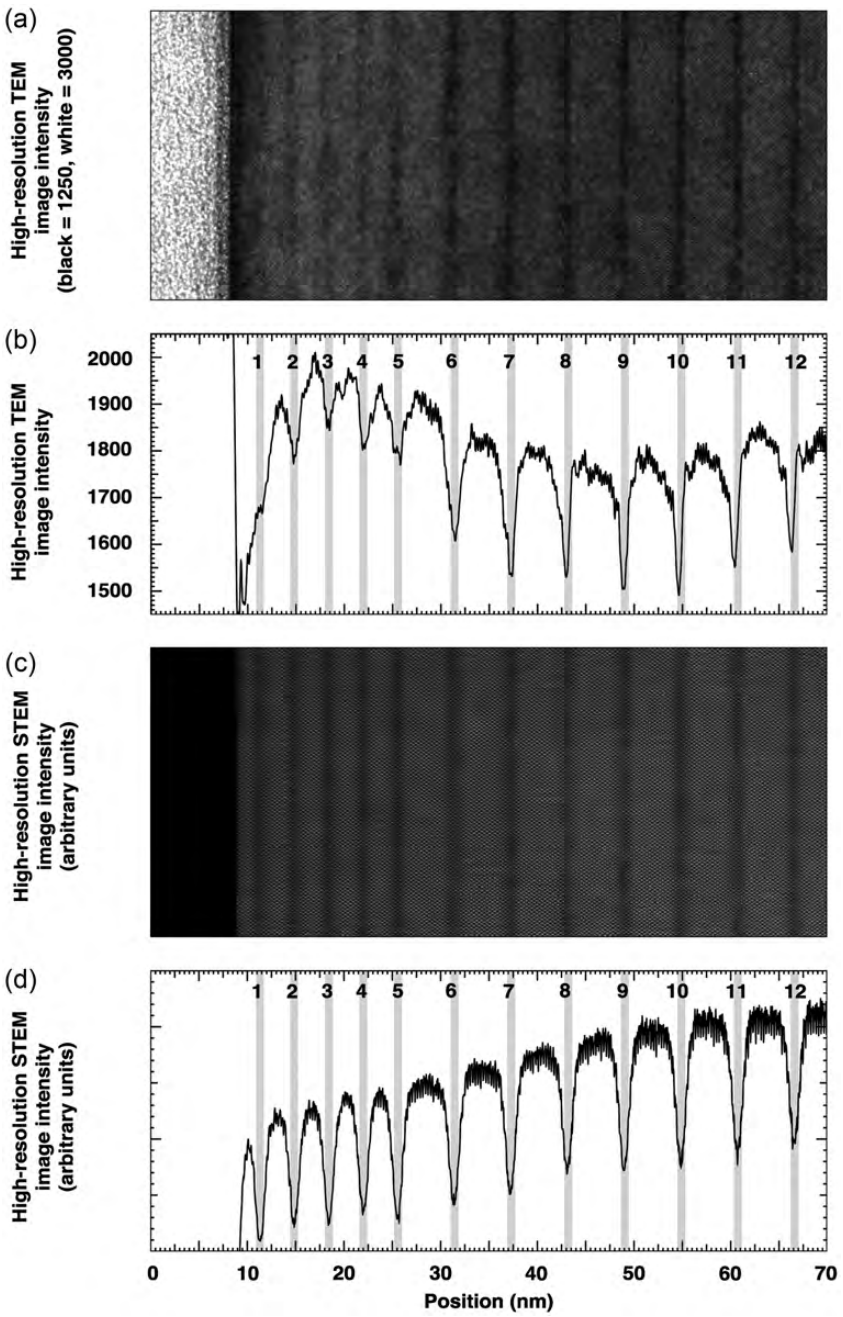


**Fig. 4.** (a) Part of a high-resolution TEM image of the delta-doped layers (black = 1250, white = 3000 counts). (b) Line profile obtained by projecting the high-resolution TEM image along the layers. (c) Part of a high-resolution STEM image of the delta-doped layers. (d) Line profile obtained by projecting the high-resolution STEM image along the layers. The high-resolution TEM and STEM images were both acquired with the specimen oriented at a <110> zone axis. (The growth direction of the layers is <001>). The positions of the layers are marked in grey on each line profile.

By using the measured values of $n_B = 0.71 \pm 0.01$, $w = 1.16 \pm 0.01$ nm and $d_c = -0.0208 \pm 0.0016$ nm, and assuming values for $V_0$ (Si) and $a_{Si}$ of 12 V [ 24] and 0.5431 nm, respectively, as well as neutral atom values for $f_{Si}$ and $f_B$ taken from Rez *et al.* [25] of 0.57535 and 0.27850 nm, respectively, Eq. (7) was used to plot a graph of the predicted mean inner potential contribution to the total potential as a function of $x$, the (unknown) fraction of B in the delta-doped layer that is substitutional rather than interstitial. This graph, whose slope depends on $n_B$ and $w$ but not on $d_c$, is shown in Fig. 6. It is immediately apparent that a wide range of (both positive and negative) values of the mean inner potential

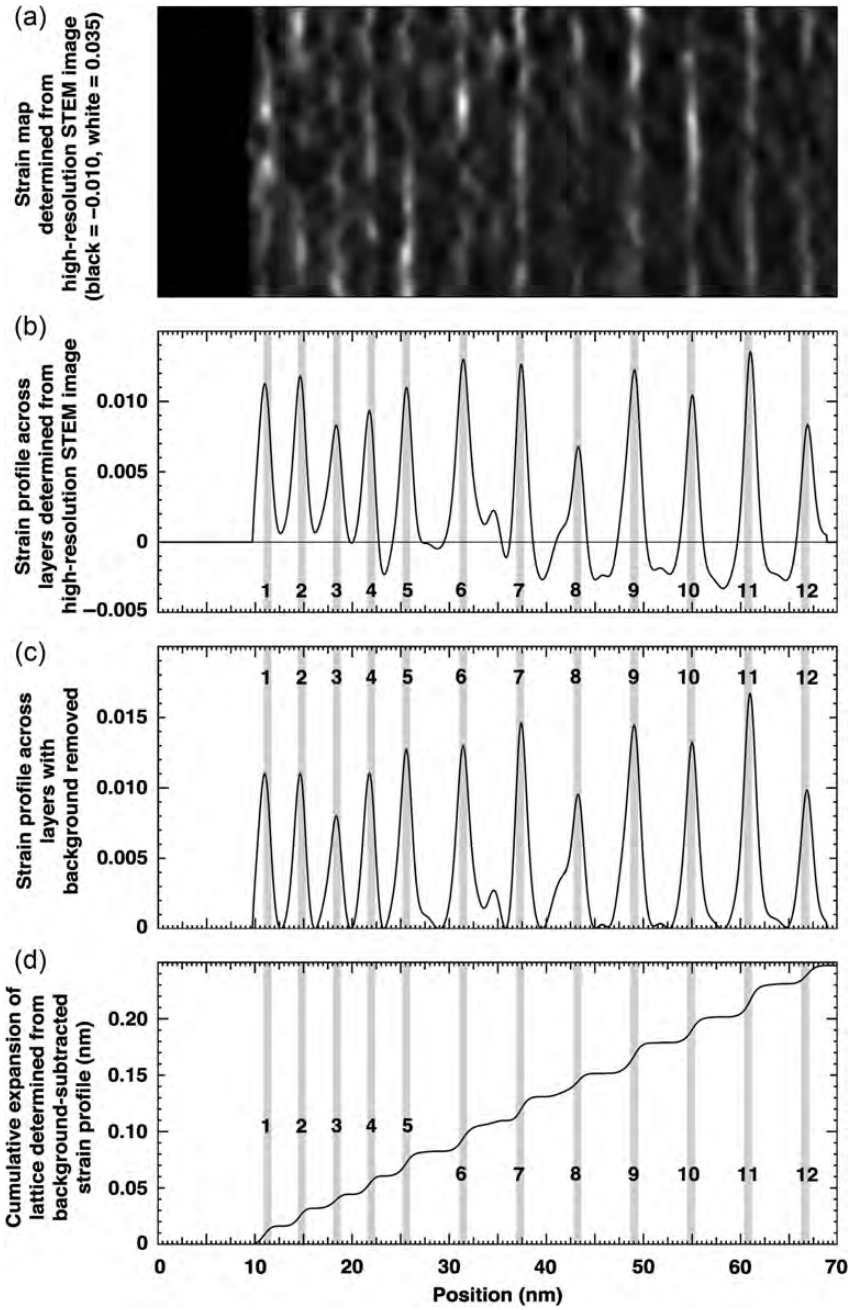


**Fig. 5.** (a) Strain map obtained by applying geometrical phase analysis to the high-resolution STEM image shown in Fig. 4c (black = –0.010, white = 0.035). Positive values in the strain map correspond to local increases in lattice parameter from that of unstrained Si, i.e. to regions of tensile strain. (b) Line profile obtained by projecting the strain map in (a) along the layers. (c) Line profile in (b) after subtracting the slowly varying background level, which is presumed to originate from scan distortions in the STEM image. (d) Cumulative expansion of the lattice determined by integrating the background-subtracted strain profile in (c) from its left-hand side. The total expansion of the lattice, from that of perfect unstrained Si, is ~0.25 nm across all 12 layers. The positions of the layers are marked in grey on each line profile.

contribution to the potential are possible, not only depending on the values of $d_c$, $n_B$ and $w$, but especially on the (unknown) fraction of B that is substitutional.

Although a value of 12 V has been used to draw the graph shown in Fig. 6, it should be noted that the absolute magnitude of $V_0$ in each part of the present specimen is unknown. As noted above, the measured change in $V_0$ between the layers and the substrate is 0.62 V. This uncertainty may introduce an error in the slope and the offset of the graph in Fig. 6 by at most 5%. This source of error

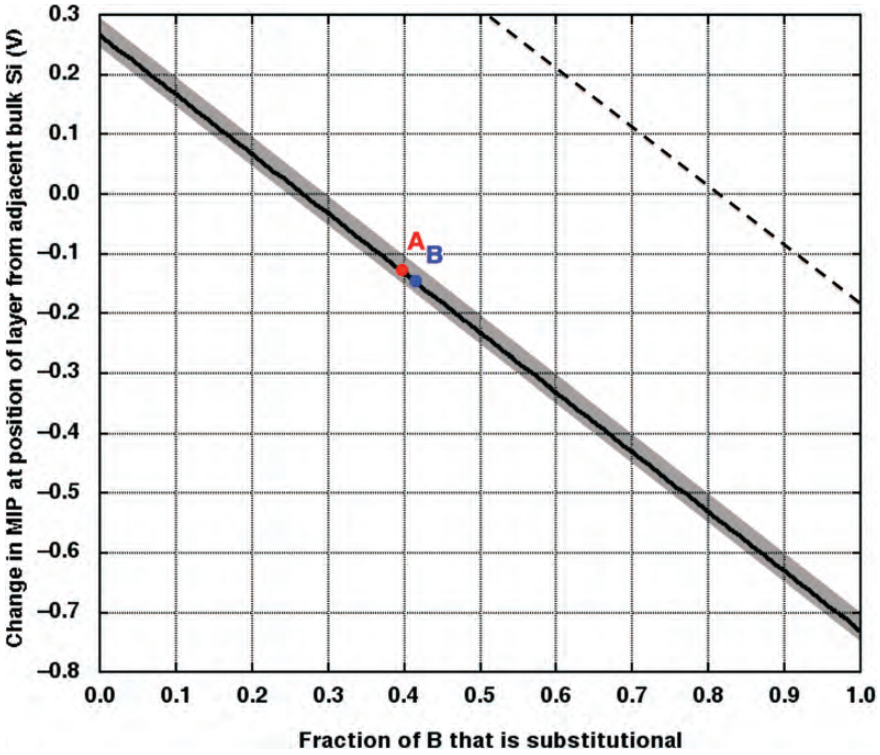


**Fig. 6.** Average mean inner potential (MIP) contribution $\Delta V_0$ to the change in potential that is predicted to be present at each delta-doped layer, based on the independent experimental measurements of total B content $n_B$, layer width $w$ and lattice shift $d_c$ presented here and plotted as a function of the fraction of B in the layer that is substitutional. The solid line and grey band represent the average values and ranges associated with the measurements given in Tables 1–3, i.e. $n_B = 0.71 \pm 0.01$ (measured from the SIMS line profile in Fig. 1), $w = 1.16 \pm 0.01$ nm (measured from the high-resolution STEM image in Fig. 4c) and $d_c = -0.0208 \pm 0.0016$ (measured from the integrated strain profile in Fig. 5d). Points A and B indicate the experimentally measured values of the average change in potential at the delta-doped layers, recorded using electron holography, before and after deconvoluting the phase profile using a Gaussian peak of width 1.15 nm, respectively (see text for details). The dashed line shows the graph that would be predicted for a value for $d_c$ of 0.032 nm (i.e. for a lattice contraction predicted using Eq. (10) for a B concentration $N_{3D}$ of $3 \times 10^{21}$ cm$^{-3}$ and a layer width $w$ of 1.16 nm, based on a lattice contraction coefficient measured for substitutional B using X-ray diffraction [26]), with all other parameters unchanged. This graph is only indicative, as the average B concentration in each layer is not precisely $3 \times 10^{21}$ cm$^{-3}$. It is also inherently only applicable to fully substitutional B, i.e. for the extreme right-hand side of the graph.

is much smaller than either the magnitude of the change in potential at each layer or the contributions to this value that are discussed in the text. It will, therefore, not be considered further.

## Discussion

Figure 6 shows that if the changes in potential that are measured experimentally from Fig. 3b are caused by the mean inner potential contribution alone, i.e. if the dopant (space charge) potential is negligible, then ~40% of the B is predicted to be substitutional and 60% interstitial. However, there are several indications that this interpretation is incorrect. First, the phase profiles measured from the layers are wider than the corresponding amplitude profiles, as would be expected for a dominant space charge contribution to the phase that is wider than the dopant distribution itself. Second, there is a lattice expansion rather than a contraction across each layer, suggesting that a significant proportion of the B is interstitial and not substitutional. If it is assumed that the B in each layer is active up to its reported solubility limit of $6 \times 10^{20}$ cm$^{-3}$ [19] and that the remaining B is interstitial, then the measured values of $n_B$ and $w$ are consistent with the presence of ~15% substitutional B and ~85% interstitial B. According to Fig. 6, this situation would correspond to a positive value of the mean inner contribution to the potential of just over 0.1 V, with the remaining −0.25 V arising from the dopant potential. If the electrically active (i.e. presumably substitutional) B concentration is only ~$10^{20}$ cm$^{-3}$, as reported by Gonzatti *et al.* [23], then the dopant contribution to the potential is predicted

to be between −0.25 V and −0.4 V. These possibilities will be considered in detail in a separate paper.

It is particularly interesting to observe that an expansion rather than a contraction of the Si lattice is measured across each layer in Fig. 5. The measured value of the lattice expansion can be compared with the lattice *contraction* that would be predicted for substitutional B alone, based on the lattice parameter of substitutional B-doped Si

$$a' = a_{\mathrm{Si}}(1 - \beta N_{3D}), \tag{8}$$

which has been measured using X-ray diffraction [26]. In Eq. (8), $N_{3D}$ is the B concentration in $\mathrm{cm}^{-3}$ and $\beta$ was measured experimentally to take a value of $5.19 \times 10^{-24}\ \mathrm{cm}^3$. For a strained layer that is constrained to match the underlying Si substrate in the plane, the lattice parameter in the layer in the growth direction can be written in the form:

$$\begin{aligned} a_{\perp} &= \left(\frac{2\upsilon}{1-\upsilon}\right)(a' - a_{\mathrm{Si}}) + a' \\ &\approx a_{\mathrm{Si}}\left[1 - \left(\frac{1+\upsilon}{1-\upsilon}\right)\beta N_{3D}\right] \end{aligned} \tag{9}$$

where $\upsilon$ is the Poisson ratio [27]. Taking a value for $\upsilon$ of 0.28 [28], Eq. (9) suggests that for solely substitutional B doping in Si, the out-of-plane lattice parameter in a delta-doped layer should be lower than that in pure Si by 2.8% for a B concentration of $3 \times 10^{21}\ \mathrm{cm}^{-3}$. The lattice contraction across a layer of width $w$ would then be given by the expression

$$d_c = \left(\frac{1+\upsilon}{1-\upsilon}\right)\beta N_{3D} w \tag{10}$$

and is predicted to take a value of 0.032 nm for a B concentration of $3 \times 10^{21}\ \mathrm{cm}^{-3}$ if $w$ is assumed to be 1.16 nm (as measured here). A dashed line in Fig. 6 shows the values of $\Delta V_0$ that would be predicted for this value of $d_c$, with all other parameters unchanged. Although this graph is only indicative, as the average B concentration in each layer is not precisely $3 \times 10^{21}\ \mathrm{cm}^{-3}$, it contrasts markedly with the predicted value of −0.73 V shown in Fig. 6 for fully substitutional B for our experimentally measured value of $d_c = -0.0208$ nm. The local change in mean inner potential that we measure for each layer is highly unlikely to be consistent with the value for $d_c$ that would be predicted for substitutional B alone. Our conclusions are that the proportion of interstitial B in our delta-doped layers is likely to be very high and that there is indeed a significant lattice expansion across each layer, rather than the lattice contraction that would be predicted for substitutional B.

## Concluding remarks

An approach has been presented for separating the mean inner potential contribution to a phase image of a highly doped semiconductor layer recorded using electron holography from the dopant potential contribution to the phase. The approach relies on an independent measurement of the total amount of dopant, the layer width and the local change in density in the doped region of the specimen and is used here to interpret a phase image recorded from 12 closely spaced delta-doped B layers in Si. The layers are sufficiently highly doped that they exhibit dark contrast in an electron holographic amplitude image, as well as in high-resolution TEM and STEM images. The fraction of the dopant that is substitutional is taken into account when comparing the predicted change in mean inner potential with the experimentally measured potential profile. Geometrical phase analysis is applied to a high-resolution STEM image of the layers and suggests that the Si lattice has undergone an expansion rather than a contraction across each layer, providing further evidence for the presence of a substantial proportion of interstitial B.

The present study has concentrated on an independent measurement of the mean inner potential contribution to the potential at a delta-doped layer. In a separate paper, we will use process simulations to determine the different possible combinations of mean inner potential and dopant potential that are consistent with the experimentally measured phase profile shown in Fig. 3b. The simulations will also be used to assess the consistency of an experimentally measured potential profile at a delta-doped layer with both predicted and measured values of the width of the free carrier wavefunction [29,30].

## Acknowledgements

Jean-Paul Barnes, Armand Béché, Chris Boothroyd, Adeline Grenier, Jean-Michel Hartmann and Pierrette Rivallin are thanked for contributions to this work.

## Funding

Financial support from a European Research Council Starting Grant (DC), a European Research Council Advanced Grant (RDB) and the European Union Seventh Framework Programme under Grant Agreement 312483 - ESTEEM2 (Integrated Infrastructure Initiative - I3) is gratefully acknowledged.

## References

1 Gabor D (1949) Microscopy by reconstructed wave-fronts. *Proc. R. Soc. A* **197**: 454–487.

2 Tonomura A (1992) Electron-holographic interference microscopy. *Adv. Phys.* **41**: 59–103.

3 Lichte H (2008) Performance limits of electron holography. *Ultramicroscopy* **108**: 256–262.

4 Dunin-Borkowski R E, McCartney M R, and Smith D J (2004) Electron holography of nanostructured materials. In: Nalwa HS (ed.), *Encyclopedia of Nanoscience and Nanotechnology*, **Vol. 3**, pp 41–100 (American Scientific Publishers).

5 Frabboni S, Matteucci G, Pozzi G, and Vanzi M (1985) Electron holographic observations of the electrostatic field associated with thin reverse-biased p–n junctions. *Phys. Rev. Lett.* **55**: 2196–2199.

6 Rau W D, Schwander P, Baumann F H, Höppner W, and Ourmazd A (1999) Two-dimensional mapping of the electrostatic potential in transistors by electron holography. *Phys. Rev. Lett.* **82**: 2614–2617.

7 Gribelyuk M A, McCartney M R, Li J, Murthy C S, Ronsheim P, Doris B, McMurray J S, Hegde S, and Smith D J (2002) Mapping of electrostatic potential in deep submicron CMOS devices by electron holography. *Phys. Rev. Lett.* **89**: 025502.

8 Twitchett A C, Dunin-Borkowski R E, Hallifax R J, Broom R F, and Midgley P A (2004) Off-axis electron holography of electrostatic potentials in unbiased and reverse biased focused ion beam milled semiconductor devices. *J. Microsc.* **214**: 287–296.

9 Twitchett A C, Dunin-Borkowski R E, Hallifax R J, Broom R F, and Midgley P A (2005) Off-axis electron holography of unbiased and reverse-biased focused ion beam milled Si p–n junctions. *Microsc. Microanal.* **11**: 66–78.

10 Twitchett A C, Yates T J V, Newcomb S B, Dunin-Borkowski R E, and Midgley P A (2007) High-resolution three-dimensional mapping of semiconductor dopant potentials. *Nano Lett.* **7**: 2020–2023.

11 Sasaki H, Yamamoto K, Hirayama T, Ootomo S, Matsuda T, Iwase F, Nakasaki R, and Ishii H (2006) Mapping of dopant concentration in a GaAs semiconductor by off-axis phase-shifting electron holography. *Appl. Phys. Lett.* **89**: 244101.

12 Cooper D, de la Peña F, Béché A, Rouvière J-L, Servanton G, Pantel R, and Morin P (2011) Field mapping with nanometer-scale resolution for the next generation of electronic devices. *Nano Lett.* **11**: 4585–4590.

13 Cooper D, Truche R, Rivallin P, Hartmann J-M, Laugier F, Bertin F, Chabli A, and Rouviere J-L (2007) Medium resolution off-axis electron holography with millivolt sensitivity. *Appl. Phys. Lett.* **91**: 143501.

14 Suzuki T, Aizawa S, Tanigaki T, Ota K, Matsuda T, and Tonomura T (2012) Improvement of the accuracy of phase observation by modification of phase-shifting electron holography. *Ultramicroscopy* **118**: 21–25.

15 Dunin-Borkowski R E, Stobbs W M, and Perovic D D (1993) The characterisation of delta doping by Fresnel contrast analysis. *Inst. Phys. Conf. Ser.* **134**: 29–32.

16 Dunin-Borkowski R E, Stobbs W M, Perovic D D, and Wasilewski Z R (1994) The interpretation of the measured mean forward scattering potential of delta–doped layers in semiconductors. In: Proceedings of the 13th ICEM, Paris, 17–22 July 1994, pp 411–412.

17 Dunin-Borkowski R E (2000) The development of Fresnel contrast analysis, and the interpretation of mean inner potential profiles at interfaces. *Ultramicroscopy* **83**: 193–216.

18 Schubert E F (1996) *Delta-doping of Semiconductors* (Cambridge University Press, Cambridge).

19 Thompson P E and Bennett J (2000) Ultrashallow junctions in silicon formed by molecular-beam epitaxy using boron delta doping. *Appl. Phys. Lett.* **77**: 2569.

20 Hÿtch M J, Snoeck E, and Kilaas R (1998) Quantitative measurement of displacement and strain fields from HREM micrographs. *Ultramicroscopy* **74**: 131–146.

21 Cooper D, Ailliot C, Barnes J-P, Hartmann J-M, Salles P, Benassayag G, and Dunin-Borkowski R E (2010) Dopant profiling of focused ion beam milled semiconductors using off-axis electron holography; reducing artefacts, extending detection limits and reducing the effects of gallium implantation. *Ultramicroscopy* **110**: 383–389.

22 Bisognin G, De Salvador D, Napolitani E, Berti M, Carnera A, Mirabella S, Romano L, Grimaldi M G, and Priolo F (2007) Substitutional B in Si: Accurate lattice parameter determination. *J. Appl. Phys.* **101**: 093523.

23 Gonzatti F, Hartmann J M, and Yckache K (2008) Low and high temperature boron and phosphorus doping of Si for junctions and MEMS purposes. *ECS Trans.* **16**: 485–493.

24 Formanek P and Kittler M (2005) Potential and limitations of electron holography in silicon research. *Solid State Phenom.* **108–109**: 603–608.

25 Rez D, Rez P, and Grant I (1994) Dirac–Fock calculations of X-ray scattering factors and contributions to the mean inner potential for electron scattering. *Acta Cryst. A* **50**: 481–497.

26 Holloway H and McCarthy S L (1993) Determination of the lattice contraction of boron-doped silicon. *J. Appl. Phys.* **73**: 103–111.

27 Zunger A and Wood D M (1989) Structural phenomena in coherent epitaxial solids. *J. Cryst. Growth* **98**: 1–17.

28 Brantley W A (1973) Calculated elastic constants for stress problems associated with semiconductor devices. *J. Appl. Phys.* **44**: 534–535.

29 Carter D J, Warschkow O, Marks N A, and McKenzie D R (2009) Electronic structure models of phosphorus δ-doped silicon. *Phys. Rev. B* **79**: 033204.

30 Ebert Ph, Landrock S, Chiu Y P, Breuer U, and Dunin-Borkowski R E (2012) Dopant mapping of Be δ-doped layers in GaAs tailored by counterdoping using scanning tunneling microscopy. *Appl. Phys. Lett.* **101**: 192103.